

Analysis of Electrical Faults and Mitigation Strategies for Double-star Induction Machines

Fayçal Hassaini^{1*}, Yacine Imaouchen², Samira Chekkal Ait Ouaret¹, Djamal Aouzellag¹, Said Aissou¹, Elyazid Amirouche¹, Samir Kennouche¹

¹ Université de Bejaia, Faculté de Technologie, Laboratoire de Maîtrise des Énergies Renouvelables (LMER), 06000 Bejaia, Algeria

² Université de Bejaia, Faculté de Technologie, Laboratoire de Génie Electrique Bejaia, 06000 Bejaia, Algérie

* Corresponding author, e-mail: faycal.hassaini@univ-bejaia.dz

Received: 07 December 2024, Accepted: 03 April 2025, Published online: 26 May 2025

Abstract

Double star electric machines are renowned for their robustness, reliability and torque quality. However, despite these advantages, they are prone to various mechanical and electrical faults. This research investigates the impact of electrical faults on double-star induction machines (DSIMs), encompassing phase-open and inter-turn short-circuit failures in both stator and rotor windings. A real *abc* framework is employed, considering both connected and unconnected neutral configurations, to accurately model the behavior of the machine under healthy and degraded conditions. Simulation results reveal that open-phase faults (OPF) lead to current imbalances, torque fluctuations, and speed variations, which can be mitigated through an intentional adjacent second-phase opening. Additionally inter-turn short-circuit faults (ITSCF) severity is found to be highly dependent on fault resistance, influencing current distortion and electromagnetic disturbances. The results demonstrate that the suitable configuration of the neutral depends on the fault type: connecting the neutral (CN) generally reduces the severity of OPF issues, whereas disconnecting the neutral (UNC) is more effective for mitigating stator ITSCF. These strategies effectively reduce disturbances and minimize torque and speed ripples, thereby maintaining optimal machine performance. Furthermore, detailed spectral analysis of DSIM signatures is performed, highlighting the complexities involved in fault diagnosis and emphasizing the importance of accurate fault identification for ensuring system reliability. These findings offer valuable insights into fault-tolerant strategies and DSIM reliability enhancement. This guarantees service continuity while keeping the main loads connected.

Keywords

double-star induction machine, open-phase fault, inter-turn short-circuit fault, connected and unconnected neutrals, fault diagnosis and mitigation

1 Introduction

Polyphase machines play a crucial role in the industrial sector, offering several advantages over conventional three-phase machines, notably in terms of power segmentation and rotor loss reduction [1]. Among these machines, double-star induction machines (DSIM) are widely used in various applications, including embedded systems and information systems [2, 3]. The DSIM stands out for its robustness, reliability, torque quality, and fault tolerance [4, 5]. In the case of a DSIM with a 30° phase shift, the offset between the two stars effectively, the offset between the two stars helps eliminate the 5th and 7th harmonics, as well as the 3 k harmonics in the case of unconnected neutrals, while reducing other harmonics at 6 k ± 1 [6]. These machines can feature squirrel-cage or wound rotors, each

with its advantages and disadvantages. In motors with wound rotors, rotor access allows control over motor torque and speed, as well as fault detection at both the rotor and stator levels. They can reach up to twice the nominal speed and power without defluxing and up to three times the nominal values with defluxing. Additionally, they can operate in degraded mode, prioritizing main loads while managing auxiliary loads, which ensures service continuity without interruption [7–10]. Despite its many advantages, the DSIM remains vulnerable to certain failures that can disrupt its operation. These malfunctions can affect both the stator and the rotor. Stator faults are generally due to electrical constraints [11, 12]. Among electrical faults, the most common in electric machines are

open-phase faults (OPF) and inter-turn short-circuit faults (ITSCF) [13]. These anomalies can lead to increased torque ripple, current imbalance, overheating, winding damage, and reduced efficiency [14]. Most studies consider the severity of ITSCF primarily related to short-circuit current amplitude, as high current accelerates the fault. A recently proposed algorithm directly determines the number of short-circuited turns in a faulty machine [15]. This approach, though promising, is limited to situations where the short circuit is already present and does not account for insulation-related failures [16–18]. Some research has explored the use of extended Kalman filters for diagnosing and identifying inter-turn short-circuit faults in the stator. Although this method is valued for its sensitivity and fast convergence, it has limitations that make it less reliable than frequency-based fault analysis [19]. Other approaches, such as reference frame transformation or the recursive Levenberg-Marquardt method, yield promising results but are complex and require substantial computational resources [20, 21]. Some studies combine discrete wavelet transforms and neural networks, despite challenges in data collection, implementation complexity, and result interpretation [22]. Certain research has focused on various types of faults that can affect winding insulation, requiring precise mathematical models of the machine and measurements of voltages and currents to detect faults and identify defective phases [10, 16]. Despite the complexity of phase-open faults, many studies have been conducted to improve fault tolerance [23–25]. Additionally, other studies tackle the OPF issue using a synchronous machine model with permanent magnets in the fifth harmonic subspace to reduce torque ripple. These works develop an advanced control algorithm requiring six PI regulators, which complicates tuning and can degrade current quality [26].

This paper presents a comprehensive study of electrical faults in the DSIms, focusing on open-phase and inter-turn short-circuit scenarios. Firstly, a real *abc* framework is employed for accurate modeling, accounting for connected and unconnected neutral configurations. This method offers a more realistic representation of machine behavior compared to traditional *dqo* transformations. Secondly, an extensive simulation analysis explores machine behavior in degraded modes, including a novel approach for open-phase fault to mitigate disturbances and maintain stable operation. The impact of neutral connections and fault resistance on performance is analyzed. Finally, detailed spectral analysis of motor signatures is investigated for the different studied scenarios.

2 Model of the wound rotor DSIM

The DSIM configuration comprises two sets of three-phase stator windings and a single three-phase rotor winding. Whose respective neutral points can either be connected or left floating. When the neutral points are connected, the machine operates in polyphase mode. At unconnected neutral, the machine in multi-star mode with a 30° offset introduces an asymmetry that eliminates the third harmonic, thus improving phase distribution, reliability and system efficiency, even in the event of a fault, compared with a conventional asynchronous machine. To simplify the modeling of this machine, magnetic saturation and eddy currents are neglected.

2.1 Electrical equations

2.1.1 Voltage equations

The machine's electrical equations for its connected neutral (CN) and unconnected neutral (UNC) operating modes are presented below in the natural reference frame (*abc*):

$$\begin{cases} [\mathbf{v}_{s1}] - [\mathbf{v}_{ns1}] = [\mathbf{r}_{s1}][\mathbf{i}_{s1}] + \frac{d[\boldsymbol{\varphi}_{s1}]}{dt} - [\mathbf{v}_{nc1}] \\ [\mathbf{v}_{s2}] - [\mathbf{v}_{ns2}] = [\mathbf{r}_{s2}][\mathbf{i}_{s2}] + \frac{d[\boldsymbol{\varphi}_{s2}]}{dt} - [\mathbf{v}_{nc2}] \\ [\mathbf{v}_r] - [\mathbf{v}_{nr}] = [\mathbf{r}_r][\mathbf{i}_r] + \frac{d[\boldsymbol{\varphi}_r]}{dt} - [\mathbf{v}_{nc}] \end{cases} \quad (1)$$

with $[\mathbf{v}_{n(s1)(s2)(r)}]$; $[\mathbf{v}_{n(c1)(c2)(c)}]$: the voltage in the various neutral sources and coils of the machine, respectively:

$$\mathbf{i}_{s1} = [\mathbf{i}_{sa1} \ \mathbf{i}_{sb1} \ \mathbf{i}_{sc1}]'; \quad \mathbf{i}_{s2} = [\mathbf{i}_{sa2} \ \mathbf{i}_{sb2} \ \mathbf{i}_{sc2}]'; \quad \mathbf{i}_r = [\mathbf{i}_{ra} \ \mathbf{i}_{rb} \ \mathbf{i}_{rc}]'$$

Expanding Eq. (1), we obtain Eq. (2):

$$\begin{cases} [\mathbf{v}_{s1}] = [\mathbf{r}_{s1}][\mathbf{i}_{s1}] + \frac{d[\boldsymbol{\varphi}_{s1}]}{dt} + [\Delta\mathbf{v}_{ns1}]\mathbf{I}_3 \\ [\mathbf{v}_{s2}] = [\mathbf{r}_{s2}][\mathbf{i}_{s2}] + \frac{d[\boldsymbol{\varphi}_{s2}]}{dt} + [\Delta\mathbf{v}_{ns2}]\mathbf{I}_3 \\ [\mathbf{v}_r] = [\mathbf{r}_r][\mathbf{i}_r] + \frac{d[\boldsymbol{\varphi}_r]}{dt} + [\Delta\mathbf{v}_{nr}]\mathbf{I}_3 \end{cases} \quad (2)$$

$$\text{with } \Delta\mathbf{v}_{ns1} = \mathbf{r}_{ns1} \left(\frac{\mathbf{i}_{sa1} + \mathbf{i}_{sb1} + \mathbf{i}_{sc1}}{i_{ns1}} \right); \quad \Delta\mathbf{v}_{ns2} = \mathbf{r}_{ns2} \left(\frac{\mathbf{i}_{sa2} + \mathbf{i}_{sb2} + \mathbf{i}_{sc2}}{i_{ns2}} \right);$$

$$\Delta\mathbf{v}_{nr} = \mathbf{r}_{nr} \left(\frac{\mathbf{i}_{ra} + \mathbf{i}_{rb} + \mathbf{i}_{rc}}{i_{nr}} \right); \quad \text{the potential differences, resistances}$$

and zeros sequences currents between the different neutrals of the stator stars and the rotor, respectively; \mathbf{I}_3 : identity matrix (3×3).

$$I_3 = \begin{bmatrix} 1 & 0 & 0 \\ 0 & 1 & 0 \\ 0 & 0 & 1 \end{bmatrix}$$

2.1.2 Magnetic equations

The magnetic equations are established in the reference frame abc [27, 28]:

$$\begin{cases} [\varphi_{s1}] = [L_{s1,s1}][i_{s1}] + [M_{s1,s2}][i_{s2}] + [M_{s1,r}][i_r] \\ [\varphi_{s2}] = [M_{s2,s1}][i_{s1}] + [L_{s2,s2}][i_{s2}] + [M_{s2,r}][i_r] \\ [\varphi_r] = [M_{r,s1}][i_{s1}] + [M_{r,s2}][i_{s2}] + [L_{r,r}][i_r] \end{cases} \quad (3)$$

The details of the inductance matrixes are defined by Eqs. (4)–(8):

$$[L_{s1,s1}] = [L_{s2,s2}] = \begin{bmatrix} L_s + L_{ms} & \frac{-L_{ms}}{2} & \frac{-L_{ms}}{2} \\ \frac{-L_{ms}}{2} & L_s + L_{ms} & \frac{-L_{ms}}{2} \\ \frac{-L_{ms}}{2} & \frac{-L_{ms}}{2} & L_s + L_{ms} \end{bmatrix} \quad (4)$$

$$[L_{r,r}] = \begin{bmatrix} L_r + L_{mr} & \frac{-L_{mr}}{2} & \frac{-L_{mr}}{2} \\ \frac{-L_{mr}}{2} & L_r + L_{mr} & \frac{-L_{mr}}{2} \\ \frac{-L_{mr}}{2} & \frac{-L_{mr}}{2} & L_r + L_{mr} \end{bmatrix} \quad (5)$$

$$[M_{s1,s2}] = L_{ms} \begin{bmatrix} \cos(\alpha) & \cos\left(\alpha + \frac{2\pi}{3}\right) & \cos\left(\alpha - \frac{2\pi}{3}\right) \\ \cos\left(\alpha - \frac{2\pi}{3}\right) & \cos(\alpha) & \cos\left(\alpha + \frac{2\pi}{3}\right) \\ \cos\left(\alpha + \frac{2\pi}{3}\right) & \cos\left(\alpha - \frac{2\pi}{3}\right) & \cos(\alpha) \end{bmatrix} \quad (6)$$

$$[M_{s1,r}] = L_m \begin{bmatrix} \cos(\theta_r) & \cos\left(\theta_r + \frac{2\pi}{3}\right) & \cos\left(\theta_r - \frac{2\pi}{3}\right) \\ \cos\left(\theta_r - \frac{2\pi}{3}\right) & \cos(\theta_r) & \cos\left(\theta_r + \frac{2\pi}{3}\right) \\ \cos\left(\theta_r + \frac{2\pi}{3}\right) & \cos\left(\theta_r - \frac{2\pi}{3}\right) & \cos(\theta_r) \end{bmatrix} \quad (7)$$

$$[M_{s2,r}] = L_m \begin{bmatrix} \cos(\theta_r - \alpha) & \cos\left(\theta_r - \alpha + \frac{2\pi}{3}\right) & \cos\left(\theta_r - \alpha - \frac{2\pi}{3}\right) \\ \cos\left(\theta_r - \alpha - \frac{2\pi}{3}\right) & \cos(\theta_r - \alpha) & \cos\left(\theta_r - \alpha + \frac{2\pi}{3}\right) \\ \cos\left(\theta_r - \alpha + \frac{2\pi}{3}\right) & \cos\left(\theta_r - \alpha - \frac{2\pi}{3}\right) & \cos(\theta_r - \alpha) \end{bmatrix} \quad (8)$$

The state system which governs the behavior of the electrical part is described by Eq. (9):

$$\begin{cases} [v_{s1}] = [r_{s1}][i_{s1}] + \frac{d}{dt}([L_{s1,s1}][i_{s1}] + [M_{s1,s2}][i_{s2}] + [M_{s1,r}][i_r]) + r_{ns1}(i_{as1} + i_{bs1} + i_{cs1})I_3 \\ [v_{s2}] = [r_{s2}][i_{s2}] + \frac{d}{dt}([M_{s2,s1}][i_{s1}] + [L_{s2,s2}][i_{s2}] + [M_{s2,r}][i_r]) + r_{ns2}(i_{as2} + i_{bs2} + i_{cs2})I_3 \\ [v_r] = [r_r][i_r] + \frac{d}{dt}([M_{r,s1}][i_{s1}] + [M_{r,s2}][i_{s2}] + [L_{r,r}][i_r]) + r_{nr}(i_{ar} + i_{br} + i_{cr})I_3 \end{cases} \quad (9)$$

where $[M_{s2,s1}] = [M_{s1,s2}]^t$, $[M_{r,s1}] = [M_{s1,r}]^t$ and $[M_{r,s2}] = [M_{s2,r}]^t$.

2.2 Electromagnetic torque equation

Electromagnetic torque is expressed in reduced form as follows:

$$T_{em} = p \left([i_{s1}]^t \frac{d}{d\theta_r} [M_{s1,r}] [i_r] + [i_{s2}]^t \frac{d}{d\theta_r} [M_{s2,r}] [i_r] \right) \quad (10)$$

2.3 Mechanical equation

The general mathematical expression for the rotational speed of a machine is given by Eq. (11):

$$J \frac{d\Omega_r}{dt} = T_{em} - T_r - f\Omega_r \quad (11)$$

3 Exposure of the DSIM models under electrical faults

DSIM are known for their efficiency. However, despite their advantages, they are subject to various electrical faults that can occur in the stator or rotor, particularly phase open faults and short circuits.

3.1 DSIM modeling with phase-opening faults

Double-star induction machines are subject to a variety of faults, including OPF, which can occur either in the stator (SOPF) or in the rotor (ROPF) (see Table A1 in the Appendix). In the case of a SOPF situation. Fig. 1 illustrates the machine's stator winding configuration in the event of a phase opening fault affecting stator phase A_{s1} . One proposed solution is to introduce a second opening phase via the switch K3, positioned at 90° to the faulty phase. The aim is to eliminate torque and speed ripples, retaining only the direct sequence component of the magnetic field. This maintains a circular rotating field in the air gap, guaranteeing smoother, more efficient machine operation.

In the case of a ROPF situation, Fig. 2 shows that the machine's rotor winding configuration, whether in normal or degraded operation, consists of a single three-phase winding, arranged in the same way as the stator winding.

A comprehensive simulation-based investigation is conducted to analyze the performance of the DSIM in degraded mode, considering open-phase conditions in both the rotor and stator. In the case of a SOPF situation, a proposed solution consists in introducing a second adjacent phase opening (OPs), defined as follows:

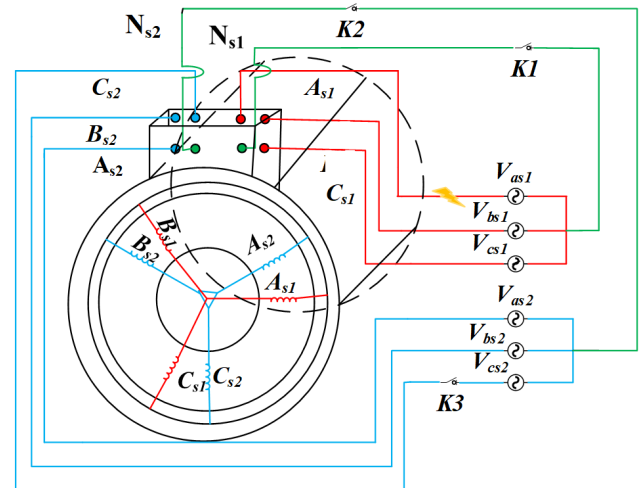


Fig. 1 Diagram presenting the two stator windings of the DSIM studied with an OPF occurring in its A_{s1} phase

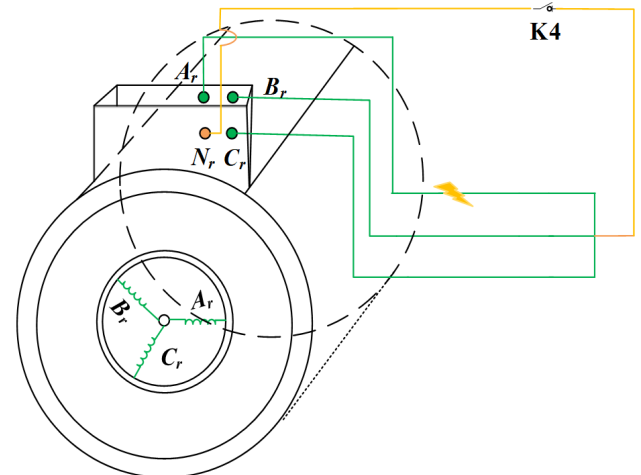


Fig. 2 Diagram showing the Rotor winding of the DSIM studied with an OPF occurring in its A_r phase

$$[r_{s1}] = \text{diag} \left([(r_{ov1} + r_{as1}) \quad r_{bs1} \quad r_{cs1}] \right) \quad (12)$$

$$[r_{s2}] = \text{diag} \left([r_{as2} \quad r_{bs2} \quad (r_{ov2} + r_{cs2})] \right) \quad (13)$$

with $r_{ov1} = r_{ov2} = \begin{cases} 0 & \text{Closed circuit} \\ \text{Very high value} & \text{Open circuit} \end{cases}$.

3.2 DSIM modeling with a short circuit fault

Previously, we studied the OPF case at stator and rotor level, considering neutral configurations (NC/UNC). At this stage, we examine the behavior of the machine in the case of ITSCF. Fig. 3 shows an explanatory diagram of the DSIM with an interturn short circuit at stator level (SITSCF), while Fig. 4 illustrates an interturn short circuit at rotor level (RITSCF).

This type of fault is more complex than the OPF, as many secondary phenomena occur in the machine. The inductance of the faulty turns depends on their relative position in the slot and the initial phase. The short-circuit current i_{rf} is added to the phase current flowing through the faulty coil, made up of short-circuited turns.

This resulting current is called the fault inductance current i_{asc} or i_{arc} . In the machine's mathematical model, the faster intervention, we diagnosed the fault using the frequency characterization method [29].

In order to model the DSIM with a short-circuit, some points were taken into consideration; the fault

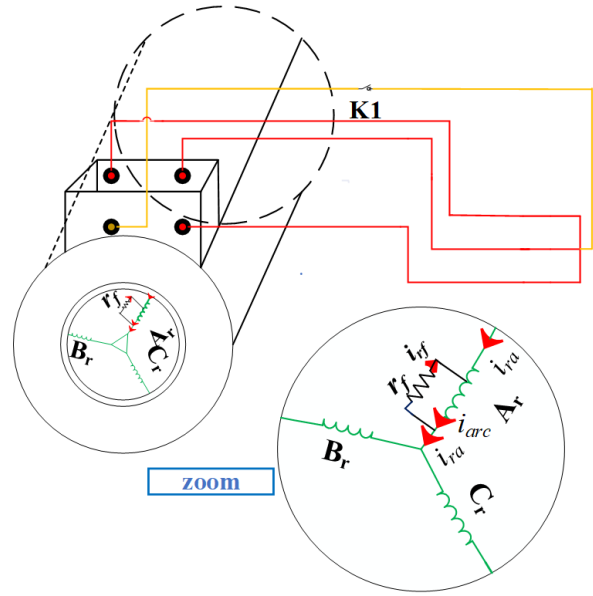


Fig. 4 Diagram illustrating the short circuit fault occurring in the rotor phase (ITSCF)

occurred in the stator on the winding of the phase A_{s1} and its resistance r_f represents a fault resistance, we take $r_f = [1000 \ 500 \ 0.5 \ 0] \ \Omega$. The coefficient μ represents the number of short-circuited turns relative to the total number of turns of the winding of phase as of the 1st star:

$$\mu = \frac{N_{asc}}{N_{as1} + N_{asc}} = \frac{N_{asc}}{N_{as}}$$

where number of turns per phase (N_{as}); N_{as1} , N_{asc} : number of turns of the two parts of the phase in short-circuit [6, 15].

In the case of ITSCF on phase A_{s1} , the electrical equation of the DSIM is defined as follows for the two cases NC or UNC.

3.2.1 Faulty DSIM model under stator ITSCF

The faulty stator resistance matrix is given by

$$[R_{s1}] = \begin{bmatrix} r & 0 & 0 & -r_f \\ 0 & r_b & 0 & 0 \\ 0 & 0 & r_c & 0 \\ -r_f & 0 & 0 & r_{ac} \end{bmatrix} \quad (14)$$

if $r = (1 - \mu)r_a + r_f$; $r_{ac} = \mu r_a$.

The stator and rotor induction matrices in the event of a stator or rotor short circuit, respectively, are as follows [30]:

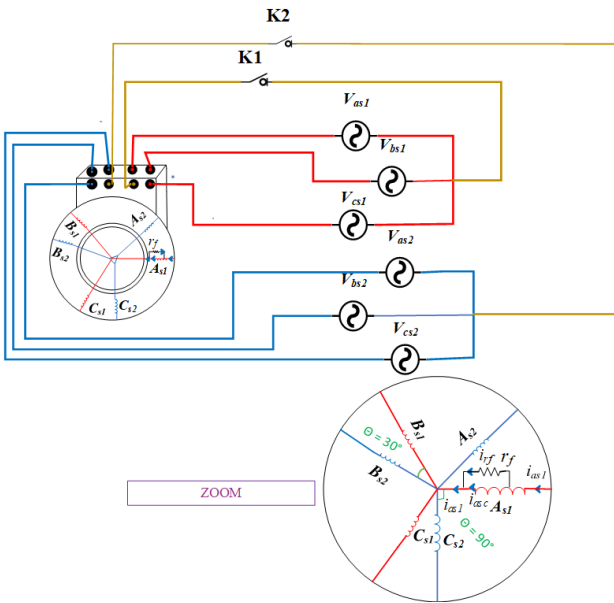


Fig. 3 Diagram illustrating the short circuit fault occurring in the stator phase (ITSCF)

$$[\mathbf{L}_{s1,s1}] = \mathbf{L}_{s1} \begin{bmatrix} (1-\mu)^2 & 0 & 0 & 0 \\ 0 & 1 & 0 & 0 \\ 0 & 0 & 1 & 0 \\ 0 & 0 & 0 & \mu^2 \end{bmatrix} + \mathbf{L}_{ms} \begin{bmatrix} (1-\mu)^2 & \frac{-(1-\mu)}{2} & \frac{-(1-\mu)}{2} & \mu(1-\mu) \\ \frac{-(1-\mu)}{2} & 1 & \frac{-1}{2} & \frac{-\mu}{2} \\ \frac{-(1-\mu)}{2} & \frac{-1}{2} & 1 & \frac{-\mu}{2} \\ \mu(1-\mu) & \frac{-\mu}{2} & \frac{-\mu}{2} & \mu^2 \end{bmatrix} \quad (15)$$

$$[\mathbf{M}_{s1,s2}] = \mathbf{L}_{ms} \begin{bmatrix} (1-\mu)\cos(\alpha) & (1-\mu)\cos\left(\alpha + \frac{2\pi}{3}\right) & (1-\mu)\cos\left(\alpha - \frac{2\pi}{3}\right) \\ \cos\left(\alpha - \frac{2\pi}{3}\right) & \cos(\alpha) & \cos\left(\alpha + \frac{2\pi}{3}\right) \\ \cos\left(\alpha + \frac{2\pi}{3}\right) & \cos\left(\alpha - \frac{2\pi}{3}\right) & \cos(\alpha) \\ (\mu)\cos(\alpha) & (\mu)\cos\left(\alpha + \frac{2\pi}{3}\right) & (\mu)\cos\left(\alpha - \frac{2\pi}{3}\right) \end{bmatrix} \quad (16)$$

where $[\mathbf{M}_{s2,s1}] = [\mathbf{M}_{s1,s2}]^t$, $[\mathbf{M}_{r,s1}] = [\mathbf{M}_{s1,r}]^t$ and $[\mathbf{M}_{r,s2}] = [\mathbf{M}_{s2,r}]^t$,

$$[\mathbf{M}_{s1,r}] = \mathbf{L}_m \begin{bmatrix} (1-\mu)\cos(\theta_r) & (1-\mu)\cos\left(\theta_r + \frac{2\pi}{3}\right) & (1-\mu)\cos\left(\theta_r - \frac{2\pi}{3}\right) \\ \cos\left(\theta_r - \frac{2\pi}{3}\right) & \cos(\theta_r) & \cos\left(\theta_r + \frac{2\pi}{3}\right) \\ \cos\left(\theta_r + \frac{2\pi}{3}\right) & \cos\left(\theta_r - \frac{2\pi}{3}\right) & \cos(\theta_r) \\ (\mu)\cos(\theta_r) & (\mu)\cos\left(\theta_r + \frac{2\pi}{3}\right) & (\mu)\cos\left(\theta_r - \frac{2\pi}{3}\right) \end{bmatrix}. \quad (17)$$

By substituting expressions Eq. (3) and Eqs. (14)–(17) into Eq. (2), we obtain the following system described in Eq. (18) in the case of stator ITSC fault.

$$\begin{cases} [\mathbf{v}_{s1}] = [\mathbf{r}_{s1}][\mathbf{i}_{s1}] + \frac{d}{dt}([\mathbf{L}_{s1,s1}][\mathbf{i}_{s1}] + [\mathbf{M}_{s1,s2}][\mathbf{i}_{s2}] + [\mathbf{M}_{s1,r}][\mathbf{i}_r]) + \mathbf{r}_{ns1}(\mathbf{i}_{as1} + \mathbf{i}_{bs1} + \mathbf{i}_{cs1} + \mathbf{i}_{asc})\mathbf{I}_3 \\ [\mathbf{v}_{s2}] = [\mathbf{r}_{s2}][\mathbf{i}_{s2}] + \frac{d}{dt}([\mathbf{M}_{s2,s1}][\mathbf{i}_{s1}] + [\mathbf{L}_{s2,s2}][\mathbf{i}_{s2}] + [\mathbf{M}_{s2,r}][\mathbf{i}_r]) + \mathbf{r}_{ns2}(\mathbf{i}_{as2} + \mathbf{i}_{bs2} + \mathbf{i}_{cs2})\mathbf{I}_3 \\ [\mathbf{v}_r] = [\mathbf{r}_r][\mathbf{i}_r] + \frac{d}{dt}([\mathbf{M}_{r,s1}][\mathbf{i}_{s1}] + [\mathbf{M}_{r,s2}][\mathbf{i}_{s2}] + [\mathbf{L}_{r,r}][\mathbf{i}_r]) + \mathbf{r}_{nr}(\mathbf{i}_{ar} + \mathbf{i}_{br} + \mathbf{i}_{cr})\mathbf{I}_3 \end{cases} \quad (18)$$

3.2.2 DSIM model under rotor ITSCF

In the case of RITSCF on phase A_r , for both cases NC or UNC.

$$[\mathbf{R}_r] = \begin{bmatrix} \mathbf{r} & 0 & 0 & -\mathbf{r}_f \\ 0 & \mathbf{r}_b & 0 & 0 \\ 0 & 0 & \mathbf{r}_c & 0 \\ -\mathbf{r}_f & 0 & 0 & \mathbf{r}_{ac} \end{bmatrix} \quad (19)$$

The submatrices of the rotor inductance matrixes are defined by Eqs. (20)–(22). By substituting expressions Eqs. (3), (6) and Eqs. (19)–(22) into Eq. (2), we obtain the system of Eq. (23) in the case of RITSCF.

$$[\mathbf{L}_{r,r}] = \mathbf{L}_r \begin{bmatrix} (1-\mu)^2 & 0 & 0 & 0 \\ 0 & 1 & 0 & 0 \\ 0 & 0 & 1 & 0 \\ 0 & 0 & 0 & \mu^2 \end{bmatrix} + \mathbf{L}_{mr} \begin{bmatrix} (1-\mu)^2 & \frac{-(1-\mu)}{2} & \frac{-(1-\mu)}{2} & \mu(1-\mu) \\ \frac{-(1-\mu)}{2} & 1 & \frac{-1}{2} & \frac{-\mu}{2} \\ \frac{-(1-\mu)}{2} & \frac{-1}{2} & 1 & \frac{-\mu}{2} \\ \mu(1-\mu) & \frac{-\mu}{2} & \frac{-\mu}{2} & \mu^2 \end{bmatrix} \quad (20)$$

$$[\mathbf{M}_{s2,r}] = \mathbf{L}_m \begin{bmatrix} (1-\mu)\cos(\theta_r - \alpha) & \cos\left(\theta_r - \alpha + \frac{2\pi}{3}\right) & \cos\left(\theta_r - \alpha - \frac{2\pi}{3}\right) & (\mu)\cos(\theta_r - \alpha) \\ (1-\mu)\cos\left(\theta_r - \alpha - \frac{2\pi}{3}\right) & \cos(\theta_r - \alpha) & \cos\left(\theta_r - \alpha + \frac{2\pi}{3}\right) & (\mu)\cos\left(\theta_r - \alpha - \frac{2\pi}{3}\right) \\ (1-\mu)\cos\left(\theta_r - \alpha + \frac{2\pi}{3}\right) & \cos\left(\theta_r - \alpha - \frac{2\pi}{3}\right) & \cos(\theta_r - \alpha) & (\mu)\cos\left(\theta_r - \alpha + \frac{2\pi}{3}\right) \end{bmatrix} \quad (21)$$

$$[\mathbf{M}_{s1,r}] = \mathbf{L}_m \begin{bmatrix} (1-\mu)\cos(\theta_r) & \cos\left(\theta_r + \frac{2\pi}{3}\right) & \cos\left(\theta_r - \frac{2\pi}{3}\right) & (\mu)\cos(\theta_r) \\ (1-\mu)\cos\left(\theta_r - \frac{2\pi}{3}\right) & \cos(\theta_r) & \cos\left(\theta_r + \frac{2\pi}{3}\right) & (\mu)\cos\left(\theta_r - \frac{2\pi}{3}\right) \\ (1-\mu)\cos\left(\theta_r + \frac{2\pi}{3}\right) & \cos\left(\theta_r - \frac{2\pi}{3}\right) & \cos(\theta_r) & (\mu)\cos\left(\theta_r + \frac{2\pi}{3}\right) \end{bmatrix} \quad (22)$$

$$\begin{cases} [\mathbf{v}_{s1}] = [\mathbf{r}_{s1}][\mathbf{i}_{s1}] + \frac{d}{dt}([\mathbf{L}_{s1,s1}][\mathbf{i}_{s1}] + [\mathbf{M}_{s1,s2}][\mathbf{i}_{s2}] + [\mathbf{M}_{s1,r}][\mathbf{i}_r]) + \mathbf{r}_{ns1}(\mathbf{i}_{as1} + \mathbf{i}_{bs1} + \mathbf{i}_{cs1})\mathbf{I}_3 \\ [\mathbf{v}_{s2}] = [\mathbf{r}_{s2}][\mathbf{i}_{s2}] + \frac{d}{dt}([\mathbf{M}_{s2,s1}][\mathbf{i}_{s1}] + [\mathbf{L}_{s2,s2}][\mathbf{i}_{s2}] + [\mathbf{M}_{s2,r}][\mathbf{i}_r]) + \mathbf{r}_{ns2}(\mathbf{i}_{as2} + \mathbf{i}_{bs2} + \mathbf{i}_{cs2})\mathbf{I}_3 \\ [\mathbf{v}_r] = [\mathbf{r}_r][\mathbf{i}_r] + \frac{d}{dt}([\mathbf{M}_{r,s1}][\mathbf{i}_{s1}] + [\mathbf{M}_{r,s2}][\mathbf{i}_{s2}] + [\mathbf{L}_{r,r}][\mathbf{i}_r]) + \mathbf{r}_{nr}(\mathbf{i}_{ar} + \mathbf{i}_{br} + \mathbf{i}_{cr} + \mathbf{i}_{arc})\mathbf{I}_3 \end{cases} \quad (23)$$

4 Results and discussion

4.1 Simulation based open-phase fault analysis

A simulation in MATLAB/Simulink [31] is conducted to observe the behavior of the variables under normal conditions and in the event of a fault. The half of the nominal mechanical torque (50 N m) is applied at $t = 1$ s.

4.1.1 Stator open-phase fault

Assuming that a single OPF appears in the A_{s1} phase and is based on the cancellation of the stator current at $t = 2$ s. As a fault-tolerant strategy, the stator current is forced to be zero in phase C_{s2} , opening the power switches of the corresponding phase at $t = 6$ s. In addition, the neutral configuration is evaluated in both cases.

The simulation results are presented in Figs. 5–9. The occurrence of the OPF initiated the deterioration in the performance of the investigated machine. This degradation is consistently characterized by unbalanced stator currents which, in turn, induce perturbations in the electromagnetic torque and mechanical speed.

The proposed reconfiguration to overcome this deterioration, by canceling the current of the C_{s2} phase (2nd phase opened), remains efficient. This action led to the stator currents adopt sinusoidal shapes, similar to their normal behavior and the curves return to their usual stable configuration for rotor currents, torque and speed.

Furthermore, the study of different neutral configurations highlights the significance of the CN in reducing

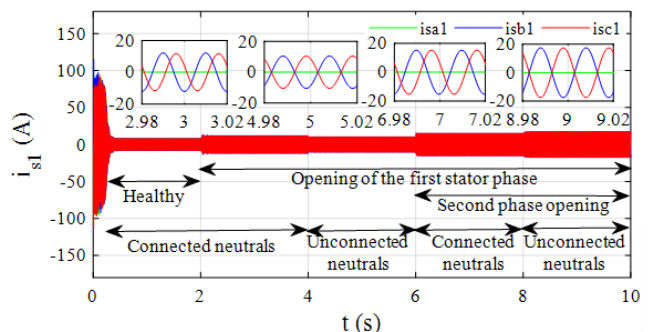


Fig. 5 1st star currents of the DSIM under the influence of the stator OPF and the neutral configuration (NC/UNC)

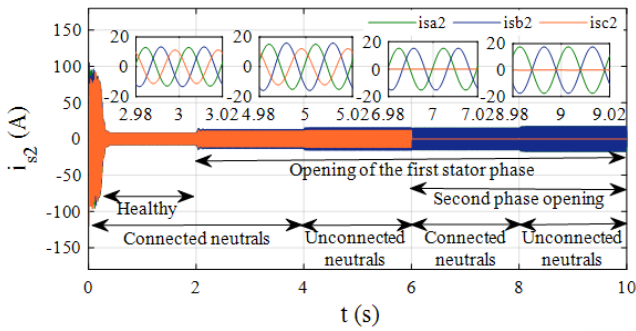


Fig. 6 2nd star currents of the DSIM under the influence of the stator OPF and the neutral configuration (NC/UNC)

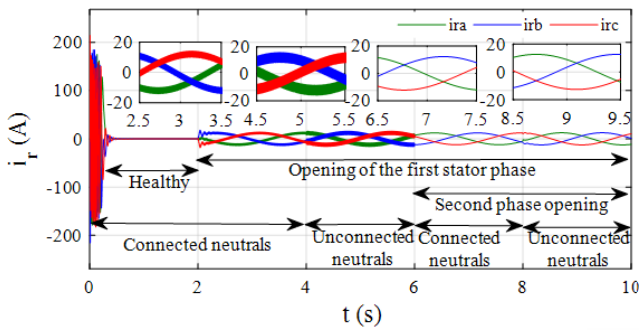


Fig. 7 Rotor currents of the DSIM under the influence of the stator OPF and the neutral configuration (NC/UNC)

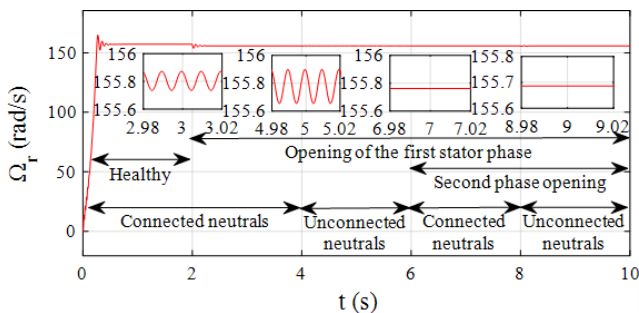


Fig. 8 Speed of the DSIM under the influence of the rotor OPF and the neutral configuration (NC/UNC)

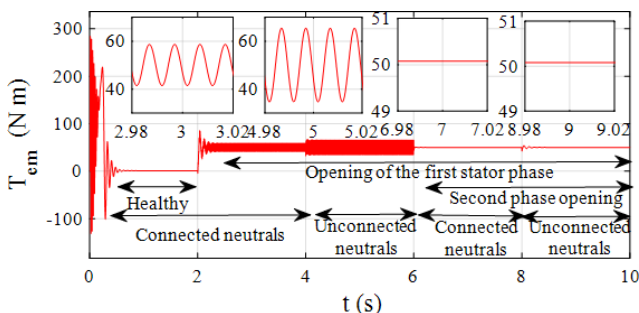


Fig. 9 Electromagnetic torque of the DSIM under the influence of the stator OPF and the neutral configuration (NC/UNC)

the severity of disturbances introduced by open-phase faults (OPFs).

Fig. 10 illustrates the machine variables spectra for the healthy case, during the stator OPF and after reconfiguration. The amplitude of the 3rd harmonic of the supply frequency ($3f_s$) in the faulty current spectrum increases compared to the healthy current. Concurrently, the amplitude of the $2f_s$ component and its harmonic of both torque and speed spectra increases proportionally to the fault severity. However, upon reconfiguration of the system to mitigate the open-phase fault, all spectra return to a profile closely similar to that of the healthy state.

The behavior of the machine variables spectra upon both neutral configurations is also investigated in the presence of the stator open-phase fault. As illustrated in Fig. 11, when using a CN configuration, there is a noticeable decrease in amplitude at faulty frequencies. This suggests that connecting the neutral is an effective method for reducing the severity of OPF issues.

4.1.2 Rotor open-phase fault

Simulations of a doubly-fed induction machine under rotor open-phase fault condition were performed, assuming a single OPF event in the A_r phase. No significant modifications to the fundamental structure of the model were required to simulate a phase disconnection; only the resistance of the affected phase was increased to a very high value, effectively simulating an open circuit. This OPF is based on the cancellation of rotor current at $t = 2$ s.

Figs. 12–16 illustrate the resulting temporal evolution of stator currents, electromagnetic torque, rotor speed, and rotor currents.

Similarly to the stator fault, when the rotor OPF occurs, the system becomes unbalanced and a high torque and speed ripples appear, which can destruct and affect the continuity of service of the system. As can be seen, those ripples are significantly higher in the unconnected neutral configuration case, reaching an amplitude of 200 N m, compared to those observed in the NC case, which do not exceed 60 N m if we compare in the healthy state their amplitude is 50 N m. These results show that it is preferable for the machine to be connected to a neutral in the case of OPF.

The spectral characteristics of stator current, torque output, and rotational velocity signals derived from a DSIM operating under rotor open-phase fault (OPF) conditions are illustrated in Fig. 17. A key indicator of a rotor fault is the appearance of sideband frequencies centered around multiples of twice slip frequency $((1 \pm 2ks)f_s)$, observable within the stator current spectrum relative to

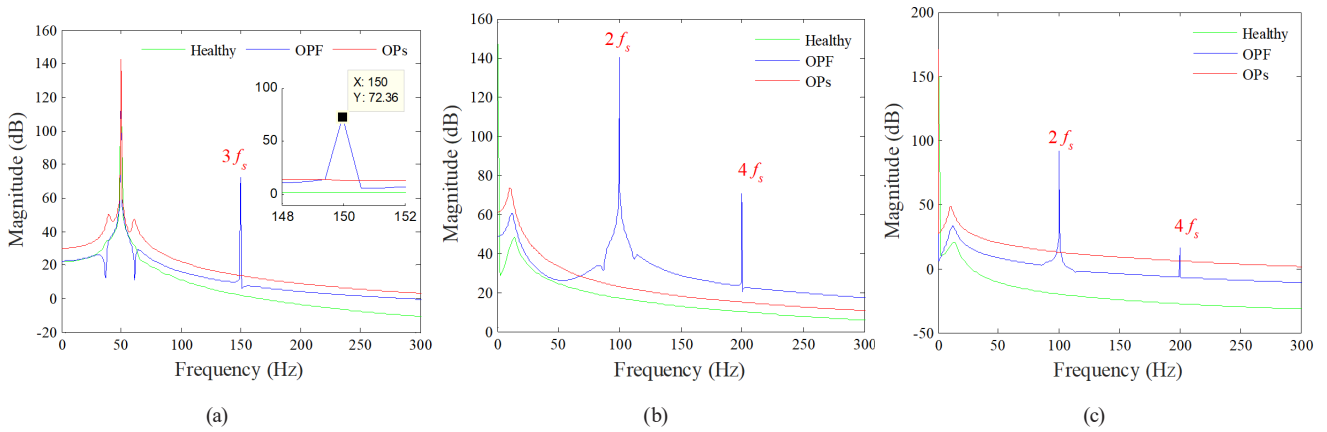


Fig. 10 Signals spectra before the stator open-phase fault, during the fault and after the reconfiguration: (a) Stator current, (b) Electromagnetic torque and (c) Speed

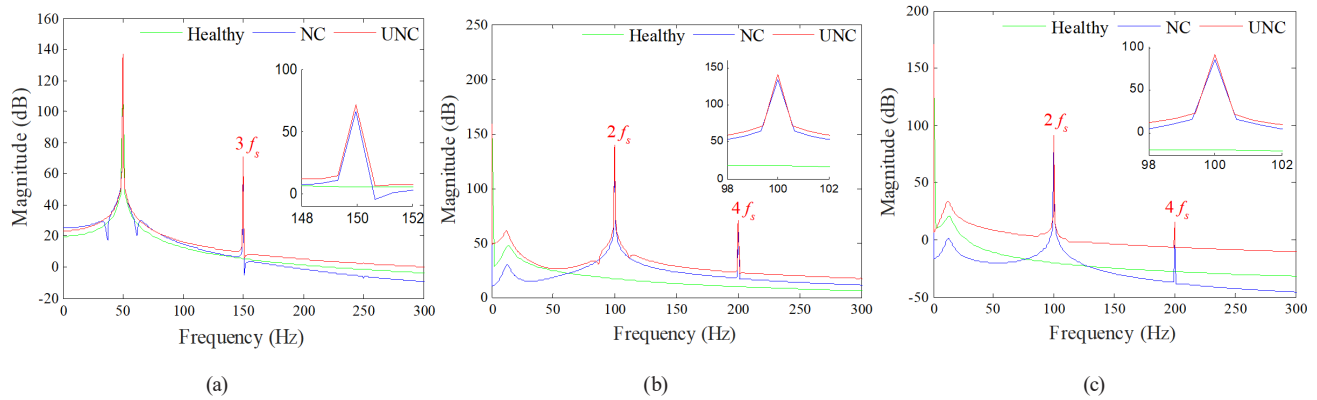


Fig. 11 Signals spectra during the OPF conditions for both neutral configurations (CN/UNC): (a) Stator current, (b) Electromagnetic torque and (c) Speed

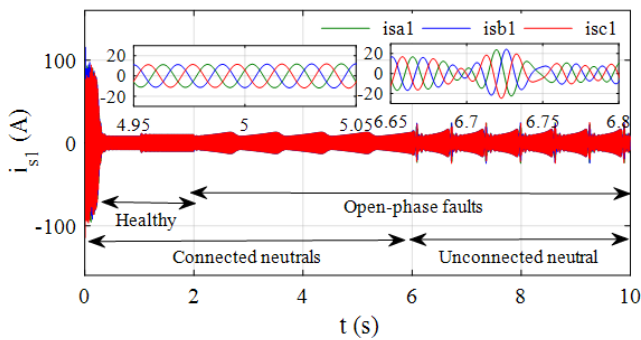


Fig. 12 1st star currents of the DSIM under the rotor OPF condition and neutral configurations (CN/UNC)

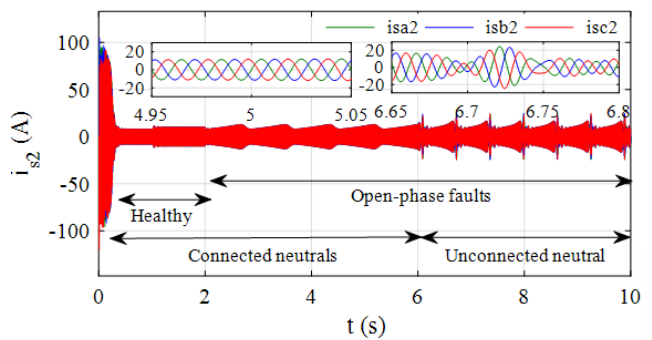


Fig. 13 2nd star currents of the DSIM under the rotor OPF condition and neutral configurations (CN/UNC)

healthy operation states. Additionally, pronounced amplitude elevations occur at twice slip frequency ($2s f_s$) along with its harmonic components across both torque and rotational velocity spectra.

Similar to the temporal evolution, these fault components exhibit lower amplitudes in the connected neutral configuration, highlighting its effectiveness in mitigating the rotor fault issues.

4.2 Simulation-based short-circuit fault analysis

A simulation in MATLAB/Simulink is conducted to observe the behavior of the variables under normal conditions and in the event of an ITSCF, as described in Section 3. The half of the nominal mechanical torque (50 N m) is also applied at $t = 1$ s.

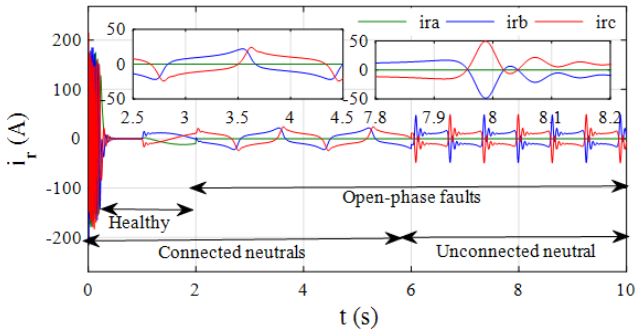


Fig. 14 Rotor currents of the DSIM under the rotor OPF condition and neutral configurations (CN/UNC)

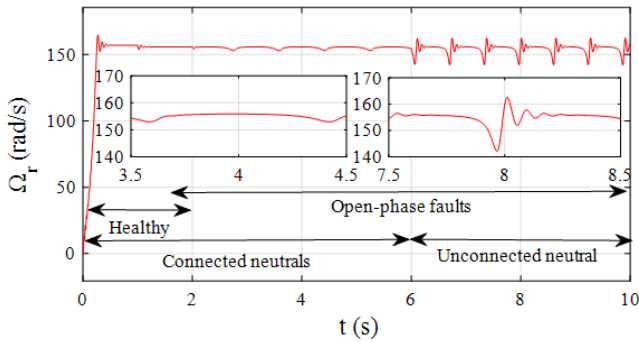


Fig. 15 Speed of the DSIM under the rotor OPF condition and neutral configurations (CN/UNC)

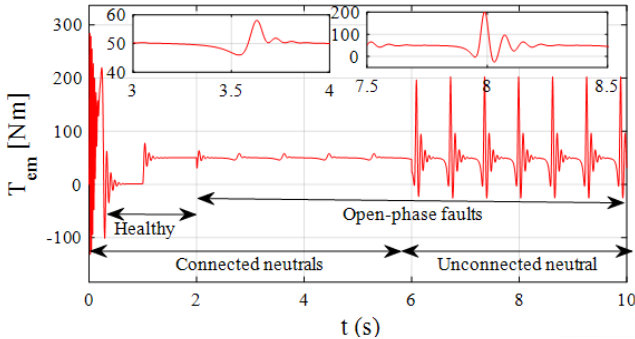


Fig. 16 Electromagnetic torque of the DSIM under the rotor OPF condition and neutral configurations (CN/UNC)

4.2.1 Stator interturn short-circuit fault

Assuming that a 15% ITSCF appears in the As1 stator phase, significant changes in the currents in the first star are observed, as shown in Fig. 18. The impact of this fault is clearly noticeable. By varying the fault resistance r_f ($r_f = 1000, 500, 0.5, \text{ or } 0 \Omega$), a fourth current, termed the short-circuit current i_{asc} , is introduced. At $r_f = 500 \Omega$, this short-circuit current has an amplitude that is considerably closer to the healthy state. When $r_f = 0.5 \Omega$, the amplitude of the i_{sb1} phase current increases by 96% compared to its healthy state, while i_{asc} increases four times compared to that recorded in the healthy condition. With $r_f = 0 \Omega$, the short-circuit current reaches a significantly higher amplitude, reaching 34 times that of the healthy state. The stator phase currents are slightly higher in this case: i_{sa1} is 4 times higher than in the healthy state, while i_{sb1} and i_{sc1} increase by 51% and 37% respectively compared with their values in the healthy state.

Fig. 19 displays the stator currents of the second star. Under NC configuration, the only notable variation occurs when $r_f = 0 \Omega$, causing a slight imbalance between phases and an increase in amplitude. In the UNC scenario, a decrease in amplitude is observed across all phases, similar to the pattern seen in the NC condition. The characteristics of rotational speed, electromagnetic torque, and rotor currents under stator ITSCF are illustrated in Figs. 20–22, where ripples appear, highlighting the impact of varying the fault resistance.

Moreover, the amplitude of these ripples increases with r_f but decreases in the UNC condition compared to the NC condition.

Fig. 23 illustrates the spectral characteristics of key machine variables during the SITSC fault occurrence. The amplitude of the third harmonic component ($3f_s$) of the

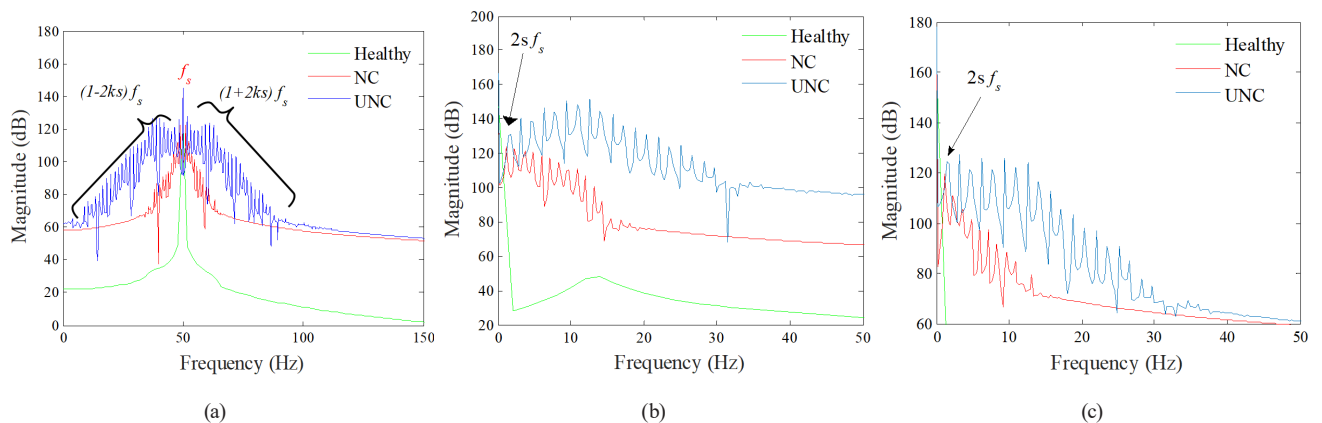


Fig. 17 Spectra of the DSIM signals under rotor OPF and neutral reconfiguration (CN/UNC):

(a) Stator current, (b) Rotor current, (c) Electromagnetic torque and (d) Speed

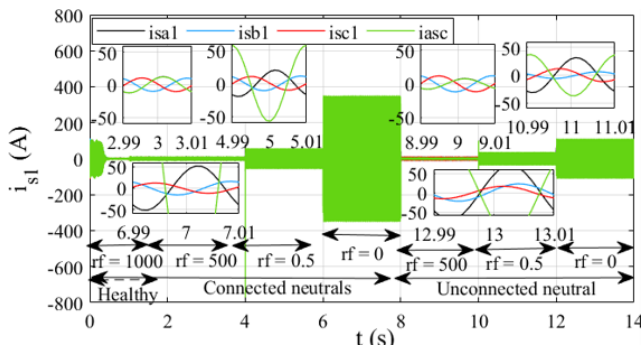


Fig. 18 Star 1 stator current in the event of a stator ITSCF with variable fault resistance and both neutral configurations (NC/UNC)

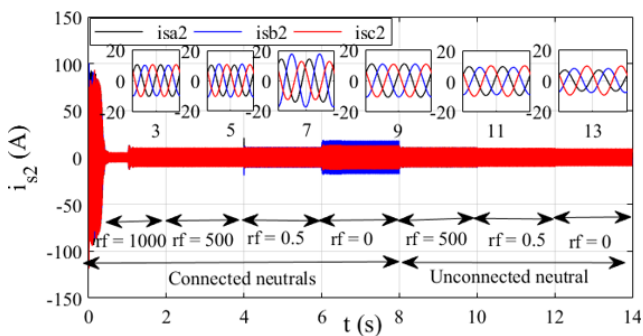


Fig. 19 Star 2 stator current in the event of a stator ITSCF with variable fault resistance and both neutral configurations (NC/UNC)

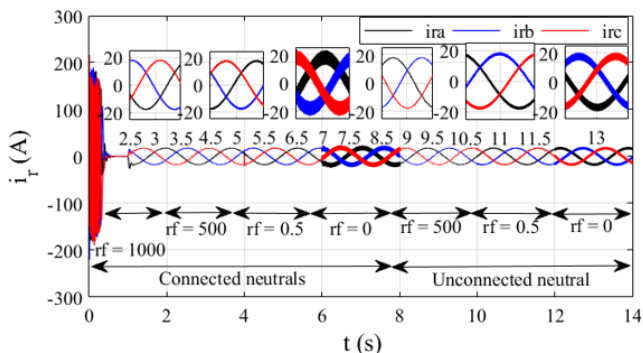


Fig. 20 Rotor current in the event of a stator ITSCF with variable fault resistance and both neutral configurations (NC/UNC)

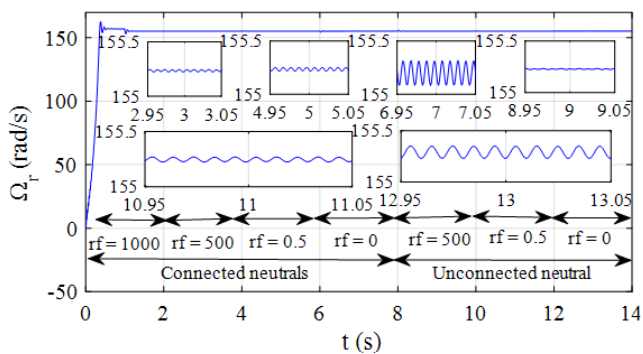


Fig. 21 Speed in the event of a stator ITSCF with variable fault resistance and both neutral configurations (NC/UNC)

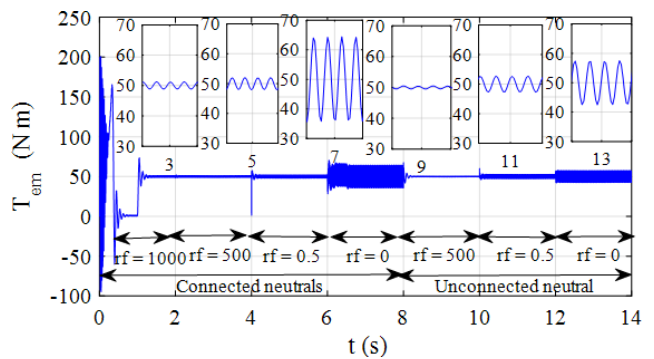


Fig. 22 Electromagnetic torque in the event of a stator ITSCF with variable fault resistance and both neutral configurations (NC/UNC)

supply frequency in the faulty current spectrum increases relative to the healthy current spectrum. Additionally, this figure reveals how these disturbances propagate through other critical parameters like torque output and rotational velocity; the amplitudes of twice the supply frequency ($2f_s$) and its harmonic ($4f_s$) increase proportionally to the fault severity.

Moreover, the spectral behavior of machine variability under two neutral configurations is also examined in response to a stator short-circuit fault. Disconnecting neutral (UNC configuration) results in a significant reduction in amplitude at the fault-related frequencies. This suggests that disconnecting the neutral provides an effective means of mitigating the severity of stator short-circuit fault issues.

4.2.2 Rotor interturn short-circuit fault

Simulations of the DSIM under the short-circuit in a rotor phase are conducted as described in the Section 3.2. The detailed representation of the temporal progression of stator and rotor current waveforms during the onset and development of the RITSCF fault can be found in Figs. 24 and 25, respectively. Despite changes in fault resistance, the time waveform of stator currents remains unchanged from the healthy state. In contrast, rotor currents exhibit an imbalance, while the torque and speed curves demonstrate oscillatory behavior, as shown in Figs. 26–28, respectively.

Therefore, connecting neutral (NC) configuration minimizes machine disturbances, leading to substantially less oscillation and better-balanced rotor currents.

The spectral analysis of the studied machine parameters under the influence of rotor ITSC fault shows harmonic components at $(1 \pm 2s)f_s$ frequencies in the stator current spectrum, as depicted in Fig. 29 (a), and their amplitudes are amplified due to the rotor fault. Additionally, both the torque and rotational velocity spectra show pronounced amplitude elevations, see Fig. 29 (a) and (b). These

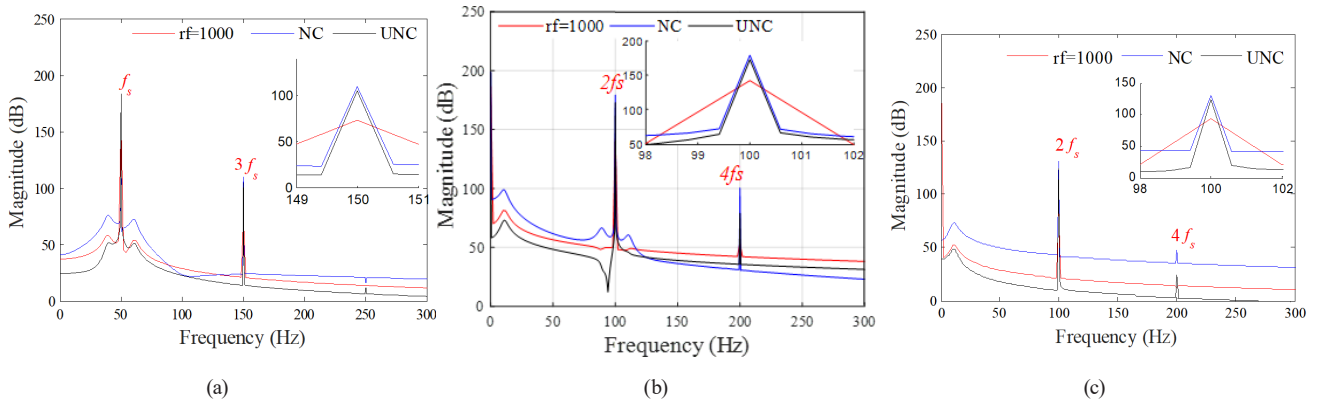


Fig. 23 Spectra of the DSIM signals under stator ITSC fault and neutral configurations (NC/UNC):
 (a) Stator current (b) Electromagnetic torque (c) rotational speed

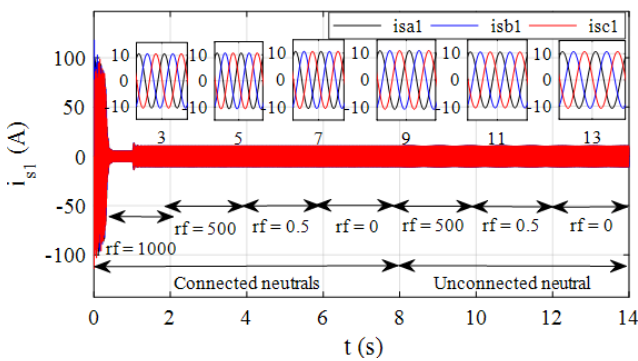


Fig. 24 Star 1 stator current in the event of a rotor ITSCF with variable fault resistance and both neutral configurations (NC/UNC)

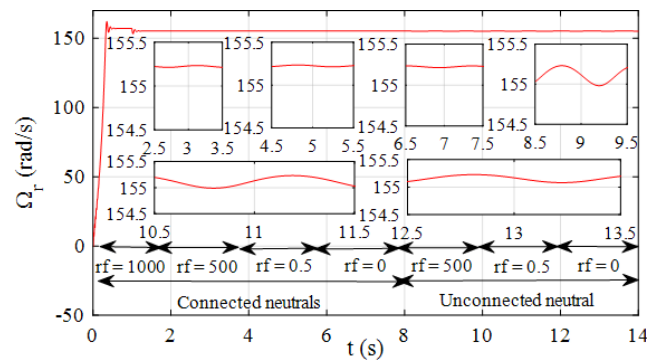


Fig. 27 Speed in the event of a rotor ITSCF with variable fault resistance and both neutral configurations (NC/UNC)

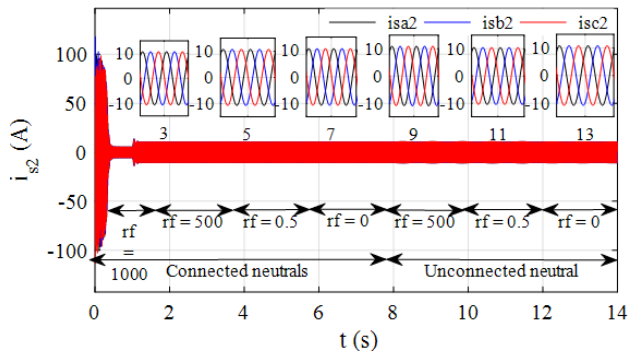


Fig. 25 Star 2 stator current in the event of a rotor ITSCF with variable fault resistance and both neutral configurations (NC/UNC)

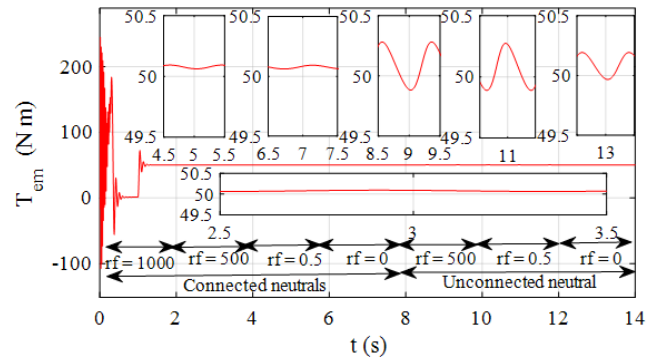


Fig. 28 Electromagnetic torque in the event of a rotor ITSCF with variable fault resistance and both neutral configurations (NC/UNC)

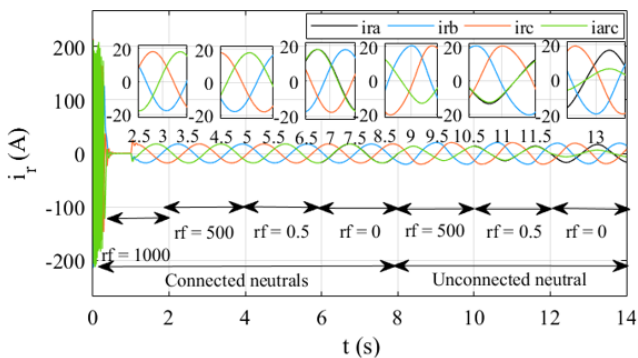


Fig. 26 Rotor current in the event of a rotor ITSCF with variable fault resistance and both neutral configurations (NC/UNC)

elevations occur at twice the supply frequency ($2s f_s$) and its harmonic components.

In contrast to the stator ITSC fault condition, disconnecting the neutral increases the amplitude at fault-related frequencies. This observation supports the conclusion that connecting the neutral is an effective way to mitigate the severity of RITSCF.

5 Conclusion

This study has provided a comprehensive analysis of electrical faults in double-star induction machines (DSIMs),

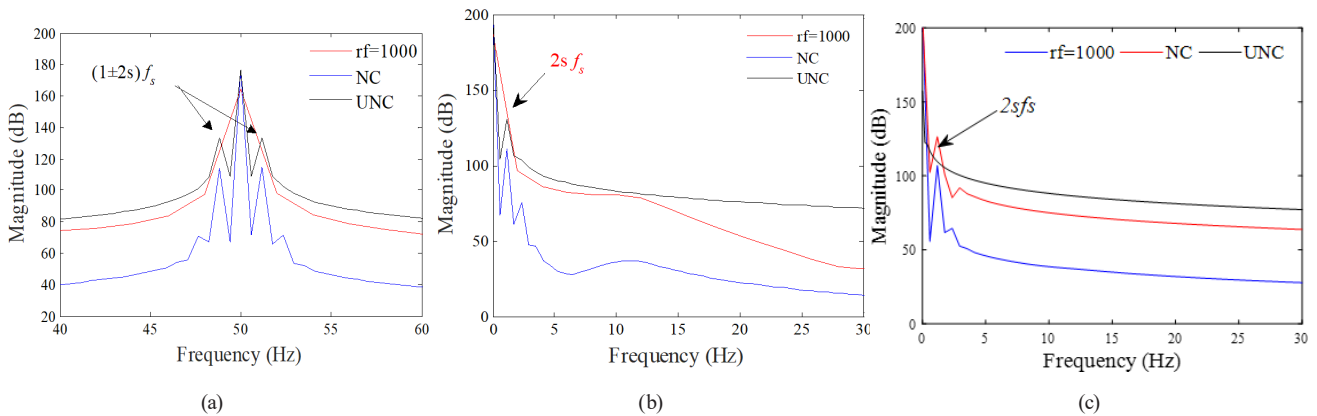


Fig. 29 Spectra of the DSIM signals under rotor ITSC fault and neutral configurations (NC/UNC):
 (a) Stator current (b) Electromagnetic torque (c) Rotational speed

focusing on open-phase faults (OPF) and inter-turn short-circuit faults (ITSCF) affecting both the stator and rotor windings. By considering both connected (CN) and unconnected neutral (UNC) configurations, we analyzed the impact of these faults on key machine parameters, including stator and rotor currents, electromagnetic torque, and rotational speed.

The simulation results indicate that OPF leads to severe imbalances in machine operation, particularly in the stator and rotor currents, inducing torque and speed fluctuations. The proposed reconfiguration strategy, involving the intentional opening of a second phase, demonstrated its effectiveness in mitigating these disturbances and restoring stable machine operation. Additionally, the study highlighted that the CN configuration helps reduce the severity of OPF-related issues, minimizing ripple effects on torque and speed.

For ITSCF, our analysis revealed that fault severity depends significantly on the fault resistance. Lower

resistance values lead to higher current imbalances, increased electromagnetic disturbances, and more pronounced harmonic components in machine signals. Spectral analysis confirmed that fault signatures manifest prominently in the frequency domain, particularly with elevated sideband frequencies and harmonics. The results further suggest that disconnecting the neutral (UNC) is beneficial in reducing the impact of stator ITSCF, whereas a connected neutral (CN) is preferable for mitigating rotor ITSCF effects.

Overall, the study underscores the crucial role of neutral configuration in fault mitigation strategies and provides valuable insights for improving DSIM reliability. Future work could focus on experimental validation of these findings and the development of advanced fault-tolerant control strategies to enhance machine performance under degraded operating conditions.

References

- [1] Adjati, A., Rekioua, T., Rekioua, D. "Degraded mode of dual stator induction motor in pumping", *Journal Européen des Systèmes Automatisés*, 53(2), pp. 273–282, 2020. <https://doi.org/10.18280/jesa.530215>
- [2] Barrera-Llana, K., Sapena-Bañó, Á., Martínez-Román, J., Puche-Panadero, R. "Implementing Deep Learning Models in Embedded Systems for Diagnosis Induction Machine", *International Journal of Electrical and Computer Engineering Research*, 3(1), pp. 7–12, 2023. <https://doi.org/10.53375/ijecer.2023.319>
- [3] Hamitouche, K., Chekkal, S., Amimeur, H., Aouzellag, D. "A New Control Strategy of Dual Stator Induction Generator with Power Regulation", *Journal Européen des Systèmes Automatisés*, 53(4), pp. 469–478, 2020. <https://doi.org/10.18280/jesa.530404>
- [4] Abdul Rahman, U. M. I. A. U., Munim, W. N. W. A., Che, H. S., Tousizadeh, M., Muhammad, K. S. "Fault tolerance of asymmetrical six-phase induction machine during single open circuit fault to three open circuit faults using GUI", *International Journal of Power Electronics and Drive Systems*, 11(2), pp. 611–617, 2020. <https://doi.org/10.11591/ijpeds.v11.i2.pp611-617>
- [5] Azib, A., Ziane, D. "A Highly Effective Modified Direct Torque Control for Five Phase Induction Motor without AC Phase Current Sensors", *Periodica Polytechnica Electrical Engineering and Computer Science*, 67(1), pp. 1–9, 2023. <https://doi.org/10.3311/PPee.20384>

- [6] Chekkal Ait Ouaret, S., Imaouchen, Y., Aouzellag, D., Ghedamsi, K. "A New Modeling Approach and Comprehensive Monitoring of Electrical Faults Through Spectral Analysis in DSIM", *Periodica Polytechnica Electrical Engineering and Computer Science*, 68(4), pp. 344–355, 2024.
<https://doi.org/10.3311/PPEe.37305>
- [7] Marques Cardoso, A. J. (ed.) "Diagnosis and Fault Tolerance of Electrical Machines", The Institution of Engineering and Technology, 2018. ISBN 978-1-78561-532-0
<https://doi.org/10.1049/PBPO126E>
- [8] Hamoudi, Y., Amimeur, H., Nacef, S. "Finite-Set Model Predictive Power Control with Common Mode Voltage Elimination for an Asymmetrical Double-Star Induction Generator Wind Energy Conversion System", *Majlesi Journal of Electrical Engineering*, 17(3), pp. 125–136, 2023.
<https://doi.org/10.30486/mjee.2023.1983159.1102>
- [9] Hamoudi, Y., Amimeur, H., Aouzellag, D., Abdolrasol, M. G. M., Ustun, T. S. "Hyperparameter Bayesian Optimization of Gaussian Process Regression Applied in Speed-Sensorless Predictive Torque Control of an Autonomous Wind Energy Conversion System", *Energies*, 16(12), 4738, 2023.
<https://doi.org/10.3390/en16124738>
- [10] Dongare, U., Umre, B., Ballal, M. "Stator inter-turn short-circuit fault diagnosis in induction motors applying VI loci-based technique", *Energy Reports*, 9(10), pp. 1483–1493, 2023.
<https://doi.org/10.1016/j.egy.2023.06.043>
- [11] Tran, C. D., Palacky, P., Kuchar, M., Brandstetter, P., Dinh, B. H. "Current and Speed Sensor Fault Diagnosis Method Applied to Induction Motor Drive", *IEEE Access*, 9, pp. 38660–38672, 2021.
<https://doi.org/10.1109/ACCESS.2021.3064016>
- [12] Khadar, S., Kouzou, A., Rezzaoui, M. M., Hafaiifa, A. "Sensorless control technique of open-end winding five phase induction motor under partial stator winding short-circuit", *Periodica Polytechnica Electrical Engineering and Computer Science*, 64(1), pp. 2–19, 2020.
<https://doi.org/10.3311/PPEe.14306>
- [13] Gherabi, Z., Benouzza, N., Bendiabdellah, A., Toumi, D. "Extension of winding function theory for modeling and diagnosis of partial demagnetization fault in pmsm drive", *Periodica Polytechnica Electrical Engineering and Computer Science* 65(3), pp. 207–217, 2021.
<https://doi.org/10.3311/PPEE.16423>
- [14] Layadi, N., Djerioui, A., Zeghlache, S., Mekki, H., Houari, A., Gong, J., Berrabah, F. "Fault-Tolerant Control Based on Sliding Mode Controller for Double-Star Induction Machine", *Arabian Journal for Science and Engineering*, 45(3), pp. 1615–1627, 2020.
<https://doi.org/10.1007/s13369-019-04120-1>
- [15] Amirouche, E., Iffouzar, K., Houari, A., Ghedamsi, K., Aouzellag, D. "Behavior analysis of dual-star permanent magnet synchronous generator with inter-turn short fault", *International Journal of Modeling and Simulation*, pp. 1–10, 2024.
<https://doi.org/10.1080/02286203.2023.2299898>
- [16] Qi, Y., Bostanci, E., Zafarani, M., Akin, B. "Severity Estimation of Interturn Short Circuit Fault for PMSM", *IEEE Transactions on Industrial Electronics*, 66(9), pp. 7260–7269, 2019.
<https://doi.org/10.1109/TIE.2018.2879281>
- [17] Zafarani, M., Bostanci, E., Qi, Y., Goktas, T., Akin, B. "Interturn short-circuit faults in permanent magnet synchronous machines: An extended review and comprehensive analysis", *IEEE Journal of Emerging and Selected Topics in Power Electronics*, 6(4), pp. 2173–2191, 2018.
<https://doi.org/10.1109/JESTPE.2018.2811538>
- [18] Maanani, Y., Menacer, A. "Modeling and diagnosis of the inter-turn short circuit fault for the sensorless input-output linearization control of the PMSM", *Periodica Polytechnica Electrical Engineering and Computer Science*, 63(3), pp. 159–168, 2019.
<https://doi.org/10.3311/PPEe.13658>
- [19] Belkhadir, A., Pusca, R., Romary, R., Belkhatat, D., Zidani, Y. "Detection of External Rotor PMSM Inter-Turn Short Circuit Fault using Extended Kalman Filter", In: 2023 IEEE 14th International Symposium on Diagnostics for Electrical Machines, Power Electronics and Drives (SDEMPED), Chania, Greece, 2023, pp. 491–497. ISBN 979-8-3503-2077-0
<https://doi.org/10.1109/SDEMPED54949.2023.10271465>
- [20] Babaa, F., Bennis, O. "An accurate inter-turn short circuit faults model dedicated to induction motors", *International Journal of Electrical and Computer Engineering*, 11(1), pp. 9–16, 2021.
<https://doi.org/10.11591/ijece.v11i1.pp9-16>
- [21] Hamoudi, A., Kouadri, B. "On-Line Stator Winding Inter-Turn Short-Circuits Detection in Induction Motors Using Recursive Levenberg-Marquardt Algorithm", *International Journal on Electrical Engineering and Informatics*, 9(1), pp. 42–57, 2017.
<https://doi.org/10.15676/ijeeci.2017.9.1.3>
- [22] Noussaiba, L. A. E., Abdelaziz, F. "ANN-based fault diagnosis of induction motor under stator inter-turn short-circuits and unbalanced supply voltage", *ISA Transactions*, 145, pp. 373–386, 2023.
<https://doi.org/10.1016/j.isatra.2023.11.020>
- [23] Gonçalves, P., Cruz, S., Mendes, A. "Finite control set model predictive control of six-phase asymmetrical machines - An overview", *Energies*, 12(24), 4693, 2019.
<https://doi.org/10.3390/en12244693>
- [24] Zhang, Z., Wu, Y., Su, H., Sun, Q. "Research on Open-circuit Fault Tolerant Control of Six-phase Permanent Magnet Synchronous Machine Based on Fifth Harmonic Current Injection", *CES Transactions on Electrical Machines and Systems*, 6(3), pp. 306–314, 2022.
<https://doi.org/10.30941/CESTEMS.2022.00041>
- [25] Liu, L., Zhang, Q. "Open-Circuit Fault-Tolerant Control of a Six-Phase Asymmetric Permanent Magnet Synchronous Motor Drive System", *Electronics*, 12(5), 1131, 2023.
<https://doi.org/10.3390/electronics12051131>
- [26] Andriamalala, R. N. "Modélisation du défaut d'excentration dans une machine asynchrone: Application au diagnostic et à la commande de deux machines spécifiques", (Modeling the eccentricity fault in an asynchronous machine: Application to the diagnosis and control of two specific machines) PhD Thesis, Université Henri Poincaré - Nancy I, 2009. [online] Available at: <https://hal.univ-lorraine.fr/tel-01748385> [Accessed: 05 December 2024] (in French)
- [27] Foito, D., Maia, J., Pires, V. F., Martins, J. F. "Double Three-phase Induction Machine Modeling for Internal Faults Simulation", *Electric Power Components and Systems*, 43(14), pp. 1610–1620, 2015.
<https://doi.org/10.1080/15325008.2015.1051634>

- [28] Iffouzar, K., Benkhoris, M.-F., Amrouche, B., Houari, A., Ghedamsi, K., Djerioui, A. "A New Post-Fault Reconfiguration Strategy under Open-Phase Operation Conditions of Asymmetrical Double-Star Induction Machines", *Energies*, 16(15), 5740, 2023. <https://doi.org/10.3390/en16155740>
- [29] Gangsar, P., Tiwari, R. "Signal based condition monitoring techniques for fault detection and diagnosis of induction motors: A state-of-the-art review", *Mechanical Systems and Signal Processing*, 144, 106908, 2020. <https://doi.org/10.1016/j.ymssp.2020.106908>
- [30] Laamari, Y., Allaoui, S., Bendaikha, A., Saad, S. "Fault Detection Between Stator Windings Turns of Permanent Magnet Synchronous Motor Based on Torque and Stator-Current Analysis Using FFT and Discrete Wavelet Transform", *Mathematical Modelling of Engineering Problems*, 8(2), pp. 315–322, 2021. <https://doi.org/10.18280/mmep.080220>
- [31] MathWorks, Inc. "MATLAB and SIMULINK, (R2015b)", [computer program] Available at: <https://www.mathworks.com/products/matlab.html> [Accessed: 30 June 2024]

Appendix

Table A1 Parameters of 15 kW double-star induction motor

Parameters	Values
Power	$P_n = 15 \text{ kW}$
Nominal frequency	$F = 50 \text{ Hz}$
Resistance of the stator winding of the first and second star	$r_{s1} = r_{s2} = 0.804 \ \Omega$
Rotor winding resistance	$r_r = 0.196 \ \Omega$
Stator leakage inductance of the first and second star	$L_s = 0.0046 \text{ H}$
Rotor leakage inductance	$L_r = 0.0032 \text{ H}$
Mutual inductance	$L_m = L_{ms} = L_{mr} = 0.0582 \text{ H}$
Number of pole pairs	$P = 2$
Viscous friction coefficient	$f = 0.0005 \text{ N m s/rad}$
Moment of inertia	$J = 0.2 \text{ kg m}^2$
Offset between two stator windings	$\alpha = 30^\circ$